Supplement of Biogeosciences, 17, 4853–4870, 2020
https://doi.org/10.5194/bg-17-4853-2020-supplement

Biogeosciences
Open Access

Supplement of

Causes and consequences of pronounced variation in the isotope composition of plant xylem water

Hannes P. T. De Deurwaerder et al.

Correspondence to: Hannes P. T. De Deurwaerder (hannes_de_deurwaerder@hotmail.com)

Method A:

Detailed description data collection French Guiana

We used data for six canopy trees and six canopy lianas sampled on two subsequent dry days (24-25 August 2017) at the Laussat Conservation Area in Northwestern French Guiana. The sampling site (05°28.604’N-053°34.250’W) lies approximately 20 km inland at an elevation of 30 m a.s.l. This lowland rainforest site has an average yearly precipitation of 2500 mm yr^{-1} (Baraloto et al., 2011). Average and maximum daily temperatures of respectively 30°C and 36°C were measured during the sampling period. Sampled individuals are located in the white sands forest habitat (Baraloto et al., 2011), on a white sandy ultisol with a typically high percentage of sand.

Individuals (Table A1) were selected based on the assessment of climbable tree, intactness of leafy canopy vegetation and close vicinity with one another to optimize similarity in meteorological and edaphic characteristics. Liana diameters were measured at 1.3 m from the last rooting point (Gerwing et al., 2006), tree diameters were measured at 1.3 m (Table A1). Liana and tree sampling allowed highly contrasted sap flux density (Gartner et al., 1990).

<u>Sampling strategy</u>

The stem xylem tissue of individual plants was sampled at different heights (1.3, 5, 10, 15, and 20 m where possible) at the same radial position of the stem, between 9:00 and 15:00 to assure high sap flow. Since upstream δ_{xyl} enrichment due to Péclet effect, in close vicinity to evaporative surfaces has been observed in the literature (Barnard et al., 2006; Dawson and Ehleringer, 1993), sampling was restricted to coring of the main stems. The order of sampling, i.e. ascending versus descending heights, was randomized. Tree stem xylem samples were collected with an increment borer (5 mm diameter), resulting in wooden cylinders from which bark and phloem tissues were removed. Coring was performed within the horizontal plane at the predefined heights, oblique to the center of the stem to maximize xylem and minimize heartwood sampling, and slowly to avoid heating the drill head and fractionation. Taking one sample generally took between 5 and 10 minutes. Since coring lianas was not possible, we collected cross-sections of the lianas after removing the bark and phloem tissue with a knife. Soil samples were collected at different depths (0.05, 0.15, 0.30, 0.45, 0.60, 0.90, 1.20, and 1.80m) within close vicinity to the sampled individuals using a soil auger. All materials were thoroughly cleaned between sampling using a dry cloth to avoid cross-contamination. Upon collection, all samples were placed in pre-weighed glass collection vials, using tweezers, to reduce contamination of the sample. Glass vials were immediately sealed with a cap and placed in a cooling box, to avoid water loss during transportation.

<u>Sample processing</u>

Sample processing was performed as in De Deurwaerder *et al.* (2018). Specifically, all fresh samples were weighed, transported in a cooler, and frozen before cryogenic vacuum distillation (CVD). Water was extracted from the samples via CVD (4 h at 105°C). Water recovery rates were calculated from the fresh weight, weight after extraction, and oven-dry weight (48 h at 105°C). Samples were removed from the analysis whenever weight loss resulting from the extraction process was below 98% (after Araguás-Araguás *et al.*, 1998). Nearly all soil samples fell below this benchmark and were therefore excluded from further analysis (Fig S1). The isotope composition of the water in the samples was measured by a Wavelength-Scanned-Cavity Ring-Down Spectrometer (WS-CRDS, L2120-i, Picarro, California, USA) coupled with a vaporizing module (A0211 High Precision Vaporizer) through a micro combustion module to avoid organic contamination (Evaristo et al., 2016; Martin-Gomez et al., 2015). Post-processing of raw δ-readings into calibrated δ-values was performed using SICalib (version 2.16; Gröning, 2011) and internal laboratory references, i.e. Lab1 (δ^2H: 7.74±0.4‰; $\delta^{18}O$: 5.73±0.06‰,), Lab3 (δ^2H: -146.98±0.4‰; $\delta^{18}O$: -20.01±0.06‰,) and quality assurance samples (δ^2H: -48.68±0.4‰; $\delta^{18}O$: -7.36±0.06‰). Calibrated δ-values are expressed on the international V-SMOW scale.

References

Araguás- Araguás, L., Froehlich, K. and Rozanski, K.: Stable isotope composition of precipitation over southeast Asia, J. Geophys. Res. Atmos., 103(D22), 28721–28742, doi:10.1029/98JD02582, 1998.

Baraloto, C., Rabaud, S., Molto, Q., Blanc, L., Fortunel, C., Herault, B., Davila, N., Mesones, I., Rios, M. and Valderrama, E.: Disentangling stand and environmental correlates of aboveground biomass in Amazonian forests, Glob. Chang. Biol., 17(8), 2677–2688 [online] Available from: https://doi.org/10.1111/j.1365-2486.2011.02432.x, 2011.

Barnard, R. L., De Bello, F., Gilgen, A. K. and Buchmann, N.: The δ18O of root crown water best reflects source water δ18O in different types of herbaceous species, Rapid Commun. Mass Sp., 20, 3799–3802, , doi:10.1002/rcm.2778, 2006.

Dawson, T. E. and Ehleringer, J. R.: Isotopic enrichment of water in the “woody” tissues of plants: implications for plant water source, water uptake, and other studies which use the stable isotopic composition of cellulose, Geochim. Cosmochim. Acta, 57(14), 3487–3492, doi:10.1016/0016-7037(93)90554-A, 1993.

De Deurwaerder, H., Hervé-Fernández, P., Stahl, C., Burban, B., Petronelli, P., Hoffman, B., Bonal, D., Boeckx, P. and Verbeeck, H.: Liana and tree below-ground water competition—evidence for water resource partitioning during the dry season, Tree Physiol., doi:10.1093/treephys/tpy002, 2018.

Evaristo, J., McDonnell, J. J., Scholl, M. A., Bruijnzeel, L. A. and Chun, K. P.: Insights into plant water uptake from xylem-water isotope measurements in two tropical catchments with contrasting moisture conditions, Hydrol. Process., 30(18), 3210–3227, doi:10.1002/hyp.10841, 2016.

Gerwing, J. J., Schnitzer, S. A., Burnham, R. J., Bongers, F., Chave, J., DeWalt, S. J., Ewango, C. E. N., Foster, R., Kenfack, D. and Martínez- Ramos, M.: A standard protocol for liana censuses, Biotropica, 38(2), 256–261, doi:10.1111/j.1744-7429.2006.00134.x, 2006.

Martin-Gomez, P., Barbeta, A., Voltas, J., Penuelas, J., Dennis, K., Palacio, S., Dawson, T. E. and Pedro Ferrio, J.: Isotope-ratio infrared spectroscopy: a reliable tool for the investigation of plant-water sources?, New Phytol., 207(3), 914–927, doi:10.1111/nph.13376, 2015.

Table A1. Sampled liana and tree individuals, provided with their species, respective diameter at breast height (DBH, in cm) and their δ^2H and $\delta^{18}O$ ranges (in ‰, VSMOW) measured per individual.

Code	Growth form	DBH [cm]	Family	Species name	δ^2H_X-range [in ‰, VSMOW]	$\delta^{18}O_X$-range [in ‰, VSMOW]
SP1	Tree	15.6	Moraceae	*Coussapoa sp.*	-30.1; -25.5	-2.8; -2.6
SP2	Tree	50.9	Fabaceae	*Vouacapoua americana*	-23.9; -18.1	-3.1; -2.2
SP3	Tree	44.6	Vochysiaceae	*Erisma nitidum*	-27.7; -20.8	-3.2; -1.9
SP4	Tree	26.1	Sapotaceae	*Micropholis guyanensis*	-29.8; -28.0	-3.0; -2.9
SP5	Tree	21.0	Anacardiaceae	*Tapirira guyanensis*	-31.1; -18.0	-3.2; -2.2
SP6	Tree	49.7	Fabaceae	*Albizia pedicellaris*	-26.9; -22.1	-3.2; -2.6
SP1	Liana	2.8	Polygonaceae	*Coccoloba sp.*	-27.9; -20.7	-3.9; -2.3
SP2	Liana	2.7	Convolvulaceae	*sp.*	-29.3; -24.0	-4.4; -2.9
SP3	Liana	0.8	Moraceae	*sp.*	-40.8; -22.6	-4.5; -2.3
SP4	Liana	3.8	Combretaceae	*cf. rotundifolium Rich.*	-23.6; -15.2	-2.9; -2.0
SP5	Liana	0.7	Convolvulaceae	*Maripa cf violacea*	-31.6; -19.7	-3.8; -2.7
SP6	Liana	3.8	Convolvulaceae	*Maripa sp.*	-35.3; -24.4	-4.8; -3.1

Method B:

Exploring the effect of diffusion on xylem transport of isotopes

The current version of the model assumes a negligible impact of diffusion on the variance in the isotopic composition of the xylem water in the stem. Here, the validity of this assumption is discussed in more detail. We will use analytical and numerical solutions of the advection-diffusion equation to simulate the transport of isotope within the xylem, followed by a short discussion.

Theory

One-dimensional solute flux (J) of a solute concentration (C) through a pipe can be expressed as the sum of the advection and diffusion processes:

$$J = uC + q \tag{1}$$

where u is the fluid flow velocity and q the diffusion flux.

The one-directional diffusion flux along the direction *x* can be expressed by Fick's law:

$$q = -D\frac{\partial C}{\partial x} \tag{2}$$

where D ($m^2\ s^{-1}$) is the diffusion constant. The mass conservation can be written:

$$\frac{\partial C}{\partial t} = -\frac{\partial J}{\partial x} \tag{3}$$

The diffusion equation

Assuming no flow ($u = 0$) and inserting (2) into (3) we obtain:

$$\frac{\partial C}{\partial t} = D\frac{\partial^2 C}{\partial x^2} \tag{4}$$

Solutions of (4) for an instantaneous point source can be given in the form

$$C(x,t) = \frac{M}{\sqrt{4\pi Dt}} exp\left(-\frac{x^2}{4Dt}\right) \tag{5}$$

where M is the mass of solute injected uniformly across the cross-section of the pipe at $x = 0$. Using the superimposition principle, we can also derive the solution for the one-dimensional stagnant case (an initial step function concentration without advection) as

$$C(x,t) = \frac{C_0}{2} erfc\left(\frac{x}{\sqrt{4\pi Dt}}\right) \tag{6}$$

where C_0 is the initial concentration at $x < 0$ and erfc is the complementary error function.

Advection-diffusion equation

In the case of flow with velocity, (4) is modified as:

$$\frac{\partial C}{\partial t} = D\frac{\partial^2 C}{\partial x^2} + u\frac{\partial C}{\partial x} \qquad (7)$$

The solution for constant concentration at $x = 0$ with initial zero concentration on a semi-infinite domain, i.e.

$$\begin{cases} C(x,0) = 0, \;\; x > 0 \\ C(0,t) = C_0, \;\; t > 0 \end{cases} \qquad (8)$$

is given by (Ogata and Banks, 1961):

$$C(x,t) = \frac{C_0}{2}\left(erfc\left(\frac{x-ut}{\sqrt{4\pi Dt}}\right) + exp\left(\frac{xu}{D}\right) erfc\left(\frac{x+ut}{\sqrt{4\pi Dt}}\right)\right) \qquad (9)$$

This solution can describe the dynamic of a solute concentration along the xylem under constant velocity, with a fixed concentration at the inlet point.

<u>Numerical solutions</u>

Solutions for problems with different boundary conditions and variable velocity are not available. In order to investigate the case with periodic concentrations at the inlet of the pipe and periodic velocity we used numerical solutions of the advection-diffusion equation

$$\frac{\partial C}{\partial t} = D\frac{\partial^2 C}{\partial x^2} + u_0 f(t)\frac{\partial C}{\partial x} \qquad (10)$$

where $f(t)$ is a periodic function. We used the wrapped normal distribution defined as

$$f(t) = \sum_{i=-100}^{i=100} \exp\left[\frac{\left(\frac{2\pi t}{24} - \pi - 2\pi k\right)^2}{2\sigma^2}\right] \qquad (11)$$

The boundary conditions at the inlet and outlet are defined as

$$\begin{cases} C = (C_{max} + C_{min})g(t) + C_{min} & x = 0, t > 0 \\ \frac{\partial C}{\partial t} = 0 & x = H, t > 0 \end{cases} \qquad (12)$$

where $g(t)$ is another periodic function defined as

$$g(t) = \sum_{i=-100}^{i=100} \exp\left[\frac{\left|\frac{2\pi t}{24} - \pi - 2\pi k\right|^3}{2\sigma^3}\right] \qquad (13)$$

The third power in (13) was chosen to match the diurnal cycle of the isotopic concentration at the tree base obtained by SWIFT. The equation was solved using the function *pdepe* implemented in Matlab (R2019a), explicitly designed to solve initial-boundary value problems for parabolic-elliptic partial differential equations in 1-D (Skeel and Berzins, 1990).

Unfortunately, numerical solutions of the advection-diffusion equation suffer numerical oscillation for values of the Péclet number greater than one (Zienkiewicz et al., 2000), so results are presented for values of diffusivity 50, 100, 200 and 400 cm^2 hr^{-1}. These values are much larger than the diffusivity of heavy water and they will produce stronger smoothing.

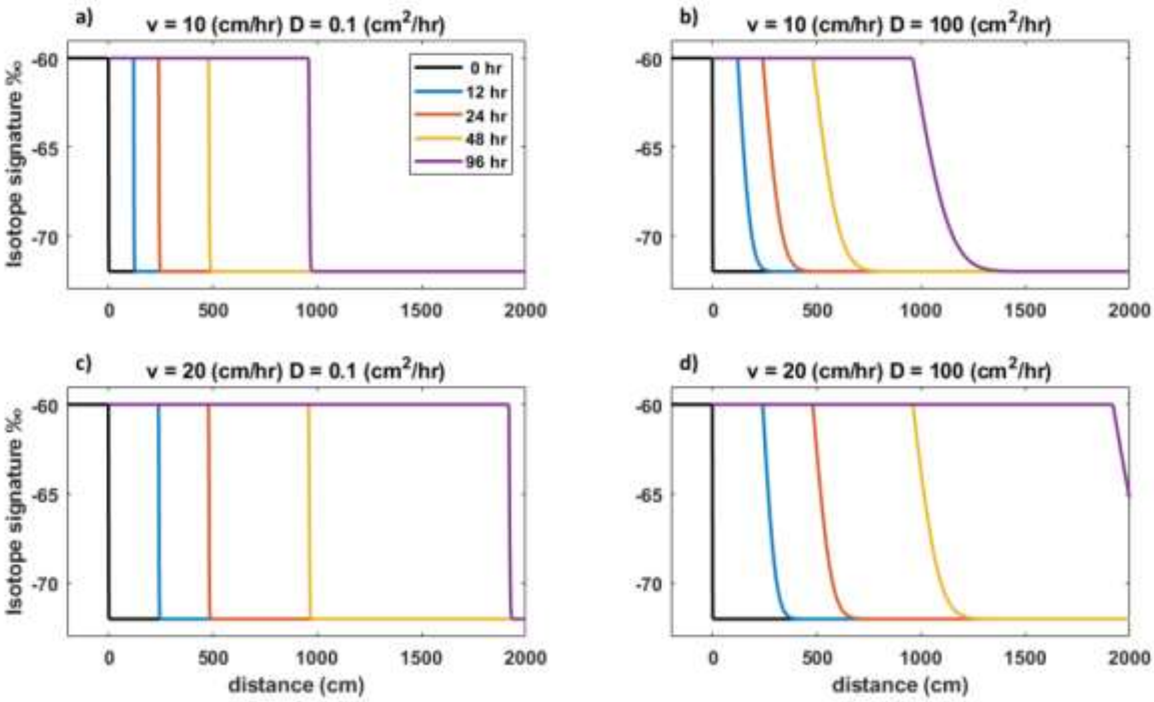

Fig B1: Analytical solutions of advection-diffusion equation on a semi-infinite 1-D domain (Eq. 9) with 12 ‰ step-change in isotope signature for different values of flow velocity and diffusivity. The plots show the impact of diffusion on the isotopic composition of xylem water. Colored lines show the solution at different time intervals: 0, 12, 24, 48, and 96 hr. Note that the values of diffusivity are much higher than these reported for heavy water (e.g. D=0.1 cm^2 h^{-1}; Meng et al., 2018)

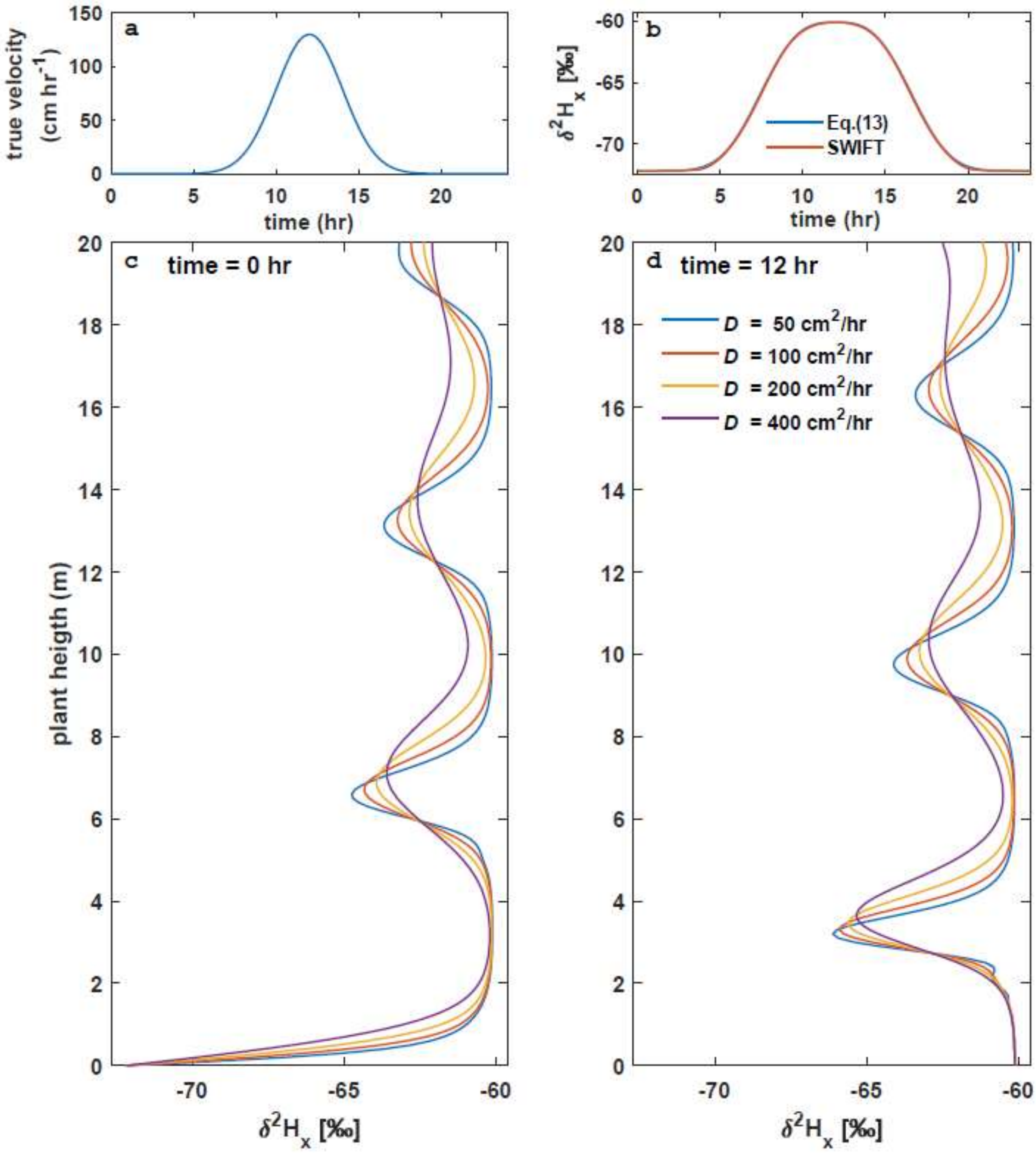

Fig B2: Numerical solutions of advection-diffusion equation on a finite 1-D domain (Eq. 10-13) with 12 ‰ step-change in isotope signature for different values of diffusivity along the length of the xylem. The periodic forcing used in the simulations are shown in panel a and b. Panels c and d show the solutions for two different time of the day. Colored lines show the solution at different diffusivity (see legend in d). Note that the values of diffusivity are much higher than these reported for heavy water (e.g. $D=0.1\ cm^2\ h^{-1}$; Meng et al., 2018).

Results and Discussion

The diffusivity of ^{2}H in water depends on temperature: at 20 ºC is D = 6.87 10^{-2} cm² hr^{-1}, at 40 ºC is D = 1.37 10^{-1} cm² hr^{-1} (Meng et al., 2018). Another process that can cause substantial mixing is the random movement of particles in the xylem network. Within each vessel, the flow is laminar, but in vessels with a larger diameter, velocity is higher than in vessels with a smaller diameter. According to the Hagen–Poiseuille law, the flow is proportional to the fourth power of diameter (hence, the velocity is proportional to diameter square). Therefore, the variable velocity experienced by the particles in the xylem network can generate substantial random motion in the transport of a solute in a similar manner of diffusion in a porous media.

Molecular diffusivity results in a relatively negligible impact of diffusion on the variance in ^{2}H when high sap flux densities are considered, as shown in Fig B1. For example, for diffusivity of 0.1 cm² hr^{-1}, after 96 hours, diffusion results in smearing in a range ± 10cm (Fig. B1a). The case with a flow velocity of 25 cm hr^{-1}, comparable to the velocity of sap in xylem, shows that the transport of the solute is minimally affected by diffusion (Fig B1 a and c). In order to appreciate the effect of diffusion, the diffusivity needs to increase three orders of magnitude (Fig B1 b and d). However, because homogenization increases with time, the impact of diffusion on δ^2H dynamics can be non-negligible for very low sap flux velocities.

Numerical solutions with the periodic forcing (Fig B2 a and b), show that for high values of diffusivity there could be a substantial smoothing in the peak (Fig B2 c and d). The smoothing progress along the path-length of the flow. However, note that a very high value of diffusivity (>400 cm^2 hr^{-1}) is required for complete homogenization above 10 m.

For the general application to isotope transport in xylem with variable input concentrations and variable sap flow velocity, diffusion can cause a smoothing of the peak and a consequent increase in the width of the δ^2H_X-baseline drop. Therefore, the probability of sampling a non-representative section within this δ^2H_X-baseline might increase, which means that neglecting diffusion could lead towards a conservative assessment of the bias in RWU estimates. However, the minimal reduction of the peak in δ^2H_X over time might lead to reducing the variability in time and space compared to the case with no diffusion. In conclusion, while diffusion does affect both the absolute range of δ^2H_X variance and the width of the δ^2H_X-baseline drop (i.e. increased probability of extracting biased samples), the impact is small in the lower part of the tree and over the timeframe and sap flow flux considered in this study. Hence, for this study, diffusion will not result in the complete homogenization of the δ^2H_X along the length of the studied trees, consistent with empirical datasets (Fig 3c, Fig S2.).

References

Meng, W., Xia, Y., Chen, Y. and Pu, X.: Measuring the mutual diffusion coefficient of heavy water in normal water using a double liquid-core cylindrical lens, Sci. Rep., 8(1), 1–7, doi:10.1038/s41598-018-30650-z, 2018.

Ogata, A. and Banks, R. B.: A solution of the differential equation of longitudinal dispersion in porous media: fluid movement in earth materials, US Government Printing Office., 1961.

Skeel, R. D. and Berzins, M.: A method for the spatial discretization of parabolic equations in one space variable, SIAM J. Sci. Stat. Comput., 11(1), 1–32, doi:10.1137/0911001, 1990.

Zienkiewicz, O. C., Taylor, R. L., Taylor, R. L. and Taylor, R. L.: The finite element method: solid mechanics, Butterworth-heinemann., 2000.

Method C:

A detailed description of the performed transport dynamics and sensitivity analyses.

Transport dynamics

The intact-root greenhouse experiment of Marshall *et al.* (2020) allows assessment if other processes besides molecular diffusivity might contribute to isotope transport through the plant, especially when very low sap flow velocities are considered. Specifically, the experiment follows the impact of a stepwise ^{2}H enrichment of the source water, i.e. from δ^2H=-59.28 ± 0.24 ‰ to δ^2H=290.57 ± 3.08‰ (see Fig 6), on the δ^2H_X dynamics in a pine tree (*Pinus pinea L.).* The tree was placed in a large pot, with the root system fully submerged in aerated water (using mini-pumps) and subjected to artificial light conditions (12h light, 12h dark, light transition at 7:00 o'clock). δ^2H_X was monitored continuously and *in situ* at two sampling heights, 0.15 cm, and 0.65 cm, respectively, using a novel borehole technique. Concomitant, sap flow velocity was measured using a sap flow sensor (heat pulse velocity sensor, Edaphic Scientific, Australia), installed at 0.85m height, and perpendicular to the upper borehole. For specific details of this experiment, we refer to Marshall *et al.* (2020).

In this setup, roots are submerged in a uniform isotopic solution, so the SWIFT model parameterization of soil and root is not necessary. The isotopic composition of the source water will, therefore, almost instantly reflect the δ^2H at the stem base. The impact of diffusion could not be considered negligible as sap flow velocities are very low (daily mean SF_V = 0.97 ± 0.39 cm h^{-1}) and the experiment lasted out 38 days before equilibrium was reached between the δ^2H_X of the source water and the δ^2H_X in both boreholes. For simulating the isotopic dynamics, we used an analytical solution of the advection-diffusion, as described in supplementary methods B, coupled to the SWIFT model. Model parameters, velocity, and diffusion were fitted by visual inspection independently for the two heights to match the initial increase in isotope signature. Note that the studied tree shows strong tapering (diam. at 0.15cm = 9.9cm; diam. at 0.65cm = 8.0cm), causing an acceleration of the sap flow along the pathway length as a same volume of water is propelled through a diminishing cross-area. This is also reflected in the allocated velocity parameters.

Sensitivity analyses

We first assessed model sensitivity to (bio)physical variables by modifying model parameters of soil type, sap flow, and root properties as compared to the standard parameterization (given in Table S1). The following sensitivity analyses were considered:

Soil type: The soil moisture content overall soil layers ($\theta_{S,i,t}$) can be deduced from the considered Meißner et al. (2012) $\Psi_{S,i,t}$ profile (see Fig. S8 and Table S1) using the Clapp & Hornberger (1978) equation:

$$\theta_{S,i,t} = \theta_{sat} \cdot \left(\frac{\Psi_{S,i,t}}{\Psi_{sat}}\right)^{-1/b} \quad (1)$$

Where θ_{sat}, Ψ_{sat} and b are soil-type specific empirical constants that correspond to sandy loam soil textures in the standard model parameterization (Clapp & Hornberger, 1978). The derived soil moisture profile ($\theta_{S,i,t}$), in turn, then provides a basis to study the impact of other soil textures. A new soil texture specific $\Psi_{S,i,t}$ profile can then be deduced by using θ_{sat}, Ψ_{sat} and b values corresponding to different soil texture types (values from Table 2 of Clapp & Hornberger (1978)). This enabled us to study $\Psi_{S,i,t}$ profiles for four distinct soil types, i.e. (i) sand, (ii) loam, (iii) sandy clay and (iv) clay soils, in relation with the original silt loam $\Psi_{S,i,t}$ profile.

Volume of water uptake: We varied the total diurnal volume of water taken up by the tree. New SF_t values are scaled using algorithms from the literature that provide an estimate of the daily sap flow volume of a tree based on its DBH (Andrade et al., 2005; Cristiano et al., 2015).

Root conductivity: We varied the root membrane permeability (k_R) to match multiple species-specific values found in the literature (Leuschner et al., 2004; Rüdinger et al., 1994; Sands et al., 1982; Steudle and Meshcheryakov, 1996).

The second set of sensitivity analyses test the impact of root hydraulics, sap flux density, and sampling strategies on the sampled $\delta^2 H_X$. We obtained 1000 samples per parameter from corresponding distributions and ranges (given in Table S2) with a Latin hypercube approach (McKay, 1988; McKay et al., 1979). This is a stratified sampling procedure for Monte Carlo simulation that can efficiently explore multi-dimensional parameter space. In brief, Latin Hypercube sampling partitions the input distributions into a predefined number of intervals (here 1000) with equal probability. Subsequently, a single sample per interval is extracted in an effort to evenly distribute sampling effort across all input values and hence reduce the number of samples needed to accurately represent the parameter space.

References

Andrade, J. L., Meinzer, F. C., Goldstein, G. and Schnitzer, S. A.: Water uptake and transport in lianas and co-occurring trees of a seasonally dry tropical forest, Trees, 19(3), 282–289, doi:10.1007/s00468-004-0388-x, 2005.

Clapp, R. B. and Hornberger, G. M.: Empirical equations for some soil hydraulic properties, Water Resour. Res., 14(4), 601–604, doi:10.1029/WR014i004p00601, 1978.

Cristiano, P. M., Campanello, P. I., Bucci, S. J., Rodriguez, S. A., Lezcano, O. A., Scholz, F. G., Madanes, N., Di Francescantonio, D., Carrasco, L. O. and Zhang, Y.-J.: Evapotranspiration of subtropical forests and tree plantations: A comparative analysis at different temporal and spatial scales, Agric. For. Meteorol., 203, 96–106, 2015.

Leuschner, C., Coners, H. and Icke, R.: In situ measurement of water absorption by fine roots of three temperate trees: species differences and differential activity of superficial and deep roots, Tree Physiol., 24(12), 1359–1367, doi:10.1093/treephys/24.12.1359, 2004.

Marshall, J. D., Cuntz, M., Beyer, M., Dubbert, M. and Kuehnhammer, K.: Borehole equilibration: testing a new method to monitor the isotopic composition of tree xylem water in situ, Front. Plant Sci., 11, 358, doi:10.3389/fpls.2020.00358, 2020.

McKay, J.: Sensitivity and uncertainty analysis using a statistical sample of input values, Uncertain. Anal., (7), pages299–314, doi:10.1007/BF01581617, 1988.

McKay, M. D., Beckman, R. J. and Conover, W. J.: Comparison of three methods for selecting values of input variables in the analysis of output from a computer code, Technometrics, 21(2), 239–245, doi:10.2307/1268522, 1979.

Rüdinger, M., Hallgren, S. W., Steudle, E. and Schulze, E.-D.: Hydraulic and osmotic properties of spruce roots, J. Exp. Bot., 45(10), 1413–1425, doi:10.1093/jxb/45.10.1413, 1994.

Sands, R., Fiscus, E. L. and Reid, C. P. P.: Hydraulic properties of pine and bean roots with varying degrees of suberization, vascular differentiation and mycorrhizal infection., Funct. Plant Biol., 9(5), 559–569, doi:10.1071/PP9820559, 1982.

Steudle, E. and Meshcheryakov, A. B.: Hydraulic and osmotic properties of oak roots, J. Exp. Bot., 47(3), 387–401, doi:10.1093/jxb/47.3.387, 1996.

Figures and tables

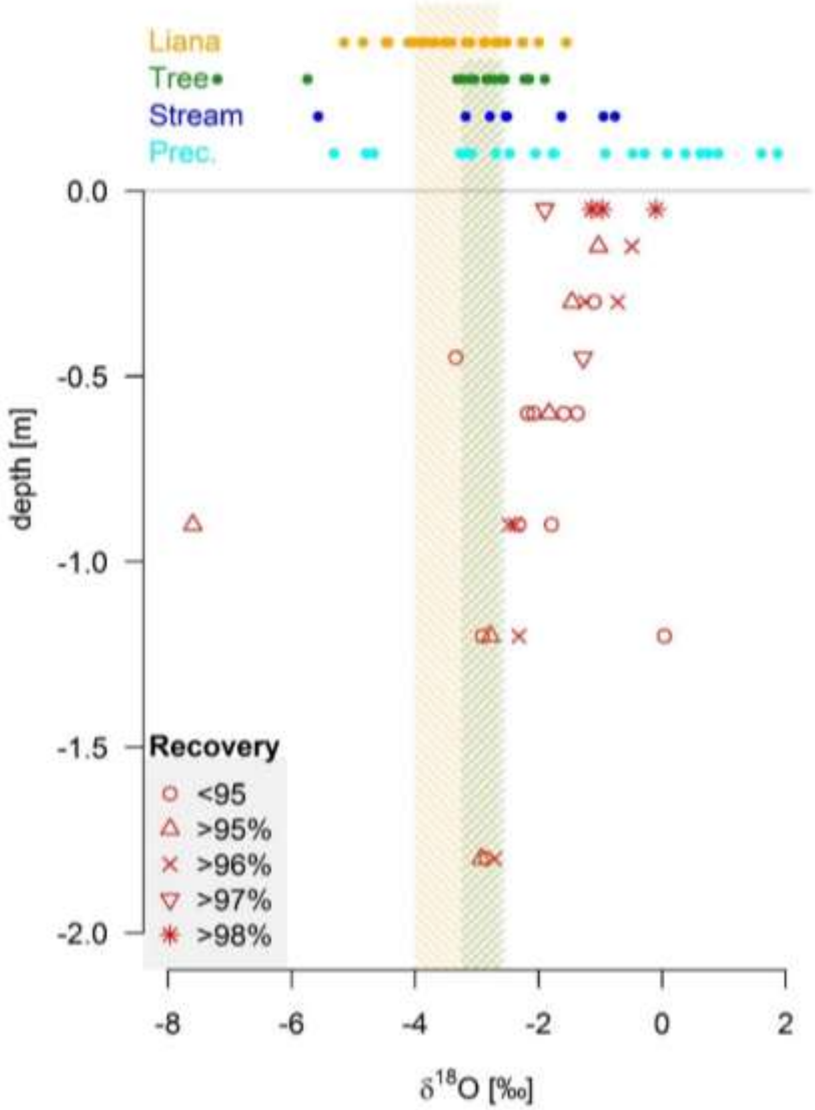

Fig. S1. Oxygen isotope composition (*$\delta^{18}O$*, in ‰ V-SMOW) of bulk soil water sampled at different depths (red), xylem water of lianas (orange) and trees (green), and from bulk stream (blue) and bulk precipitation water (cyan) in Laussat, French Guiana. Different soil *$\delta^{18}O$* composition symbols indicate the extraction recovery rates, where 98% presents the generally pursued benchmark. Shaded areas show the Q25-Q75 intervals for lianas and trees in orange and green respectively.

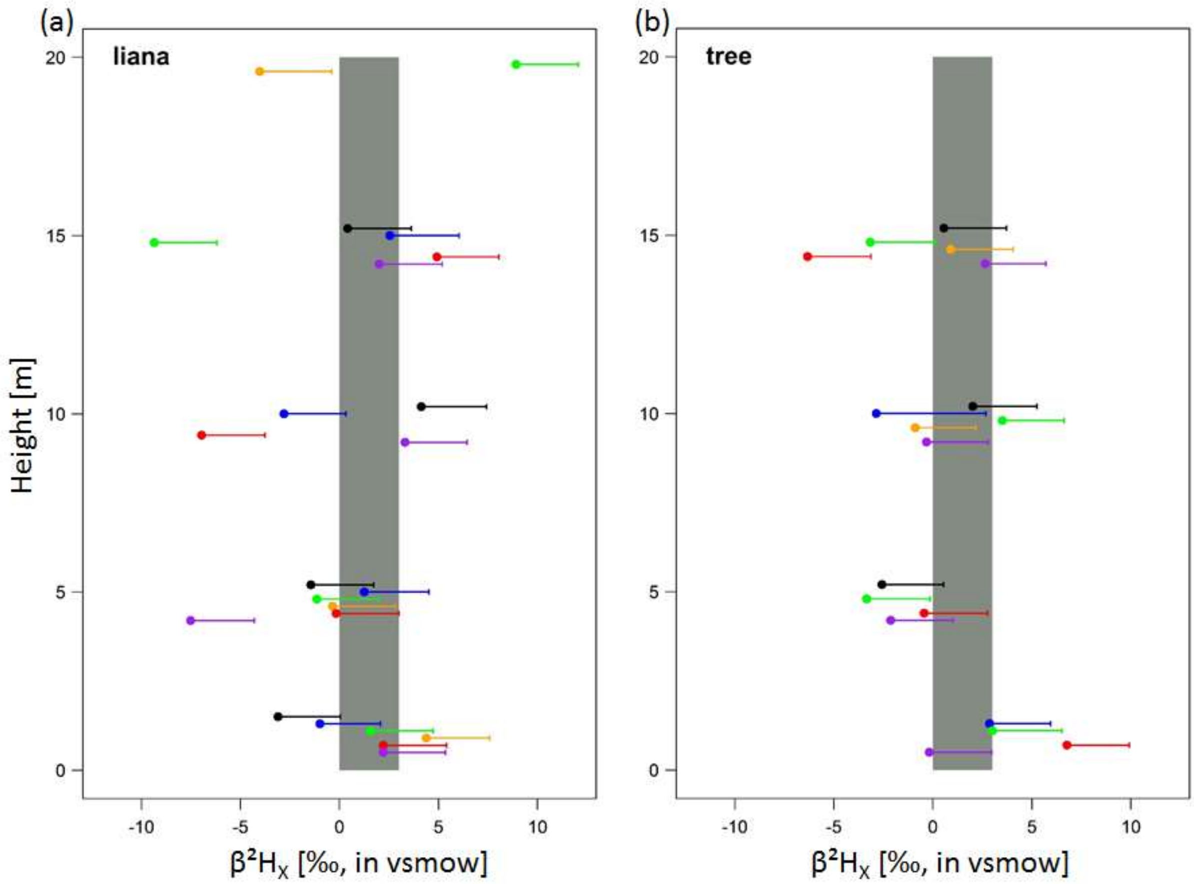

Fig. S2. Field measurements of normalized intra-individual $\delta^2 H_X$ ($\beta^2 H_X$) for six lianas (panel a) and six trees (panel b). Individuals are provided in different colors; liana species: ■ *Coccoloba sp.*, ■ sp.2, ■ sp.3, ■ *cf. rotundifolium Rich.*, ■ *Maripa cf violacea*, ■ *Maripa sp.*; tree species: ■ *Coussapoa sp.*, ■ *Vouacapoua americana*, ■ *Erisma nitidum*, ■ *Micropholis guyanensis*, ■ *Tapirira guyanensis*, ■ *Albizia pedicellaris*. Error whiskers are the combination of potential extraction and measurement errors of the isotope analyzer. The former presents a positive skew-normal distribution $SN_{empirical}(\xi = 0‰, \omega = 3‰, \alpha = +\infty)$. The full grey envelope delineates the acceptable variance from the stem mean (i.e. 3‰) according to the standard assumption of no variance along the length of a lignified plant, i.e the null model.

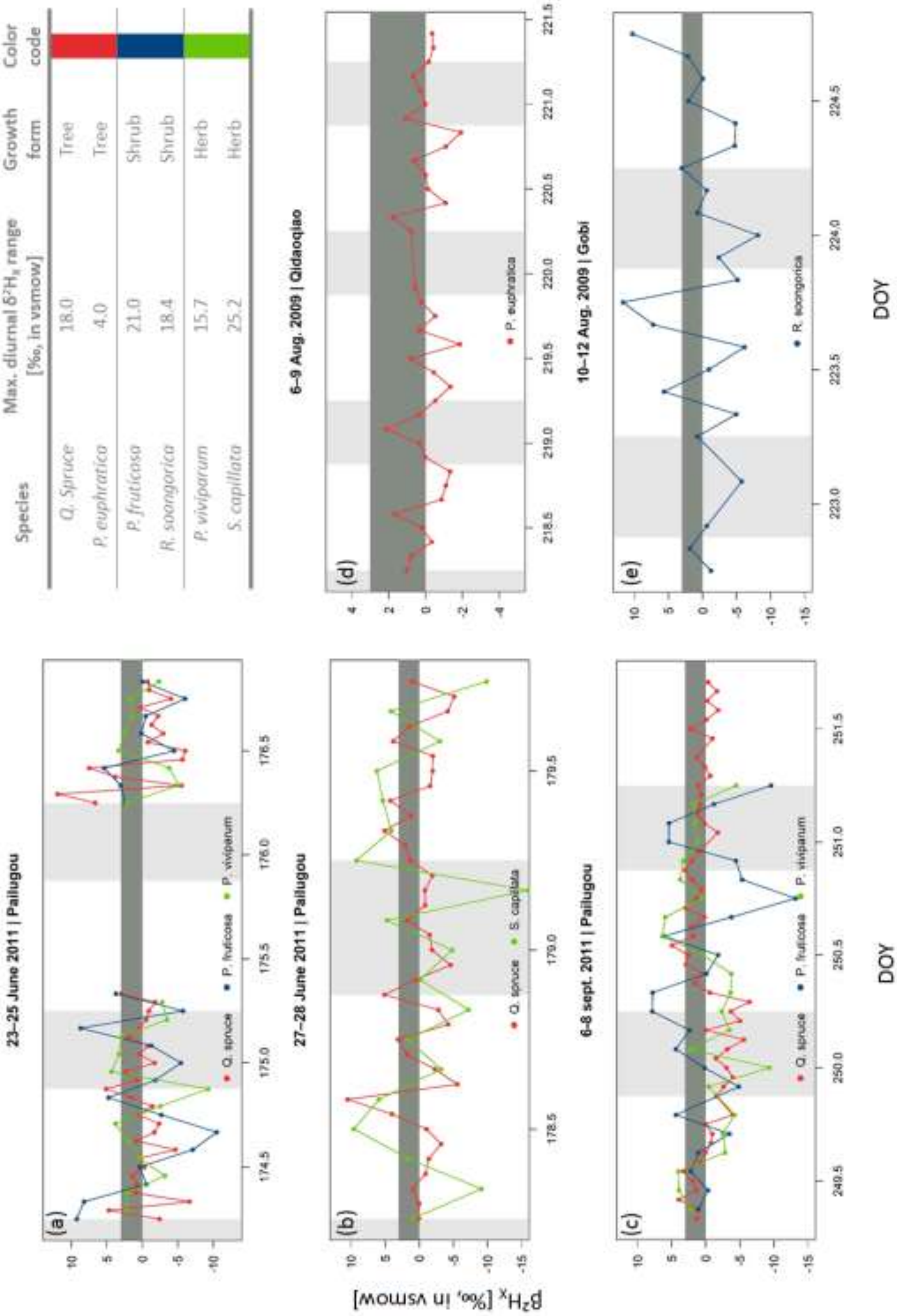

Fig. S3. High temporal field measurements of normalized δ^2H composition of xylem water (β^2H_X) of two trees (red, stem samples), two shrubs (blue, stem samples) and two herbs (green, root samples) species sampled in the Heihe River Basin (northwestern China) shown for the respective measurement periods. Timing and location of sampling are provided in the panel titles. Horizontal dark grey colored envelope delineates the acceptable variance from the stem mean (i.e. 3‰) according to the standard assumption of no variance along the length of a lignified plant. Light grey vertical envelopes mark the nighttime periods. The table provides the maximum measured diurnal δ^2H_X range per species.

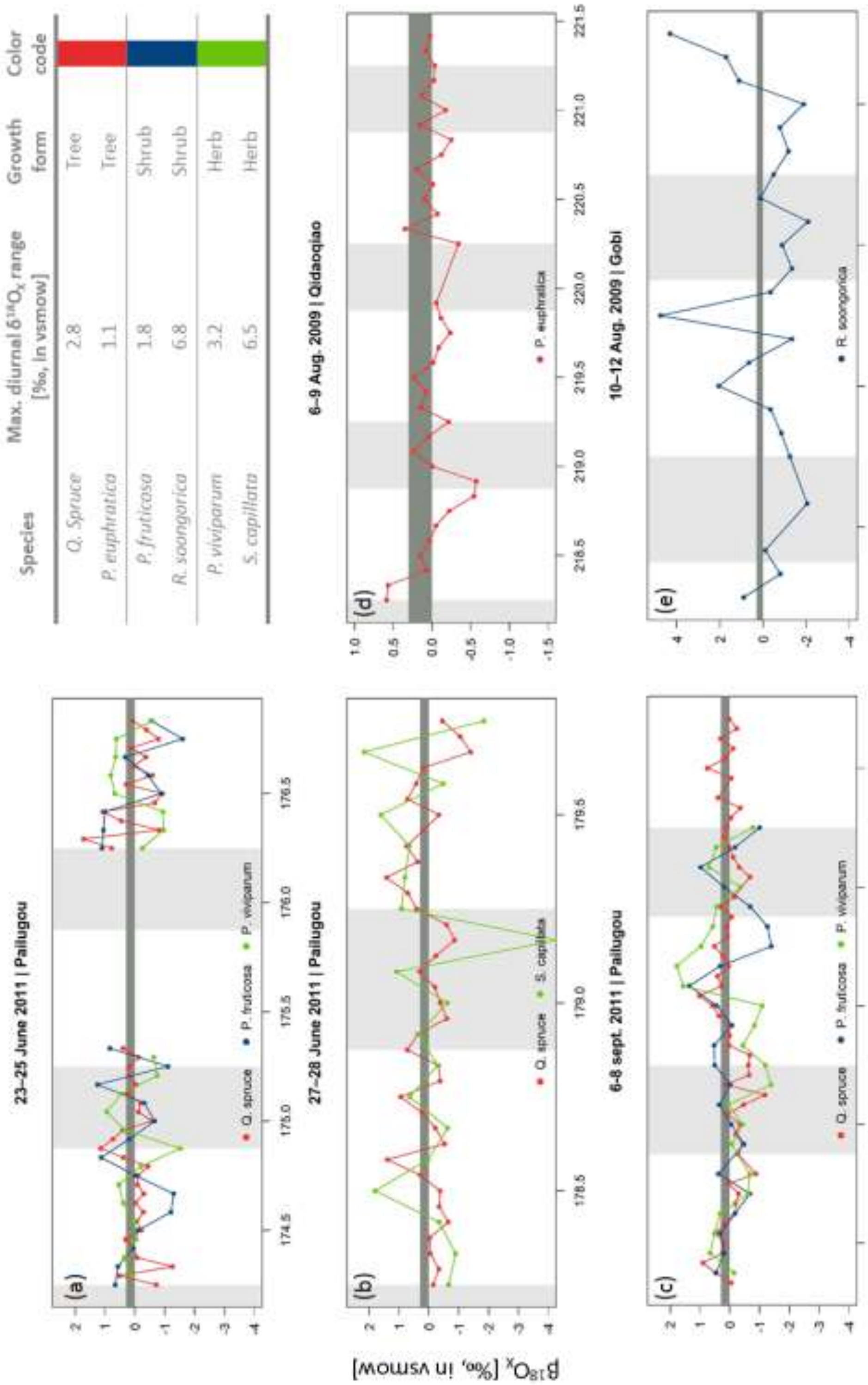

Species	Max. diurnal $\delta^{18}O_X$ range [‰, in vsmow]	Growth form	Color code
Q. Spruce	2.8	Tree	
P. euphratica	1.1	Tree	
P. fruticosa	1.8	Shrub	
R. soongorica	6.8	Shrub	
P. viviparum	3.2	Herb	
S. capillata	6.5	Herb	

Fig. S4. High temporal field measurements of normalized $\delta^{18}O$ composition of xylem water ($\beta^{18}O_X$) of two trees (red, stem samples), two shrubs (blue, stem samples) and two herbs (green, root samples) in the Heihe River Basin (northwestern China) shown for the respective measurement period. Timing and location of sampling are provided in the panel title. Horizontal dark grey colored envelope delineates the acceptable variance from the stem mean (i.e. 0.3‰) according to the standard assumption of no variance along the length of a lignified plant. Light grey vertical envelopes mark the nighttime periods. The table provides the maximum measured diurnal $\delta^{18}O_X$ range per species.

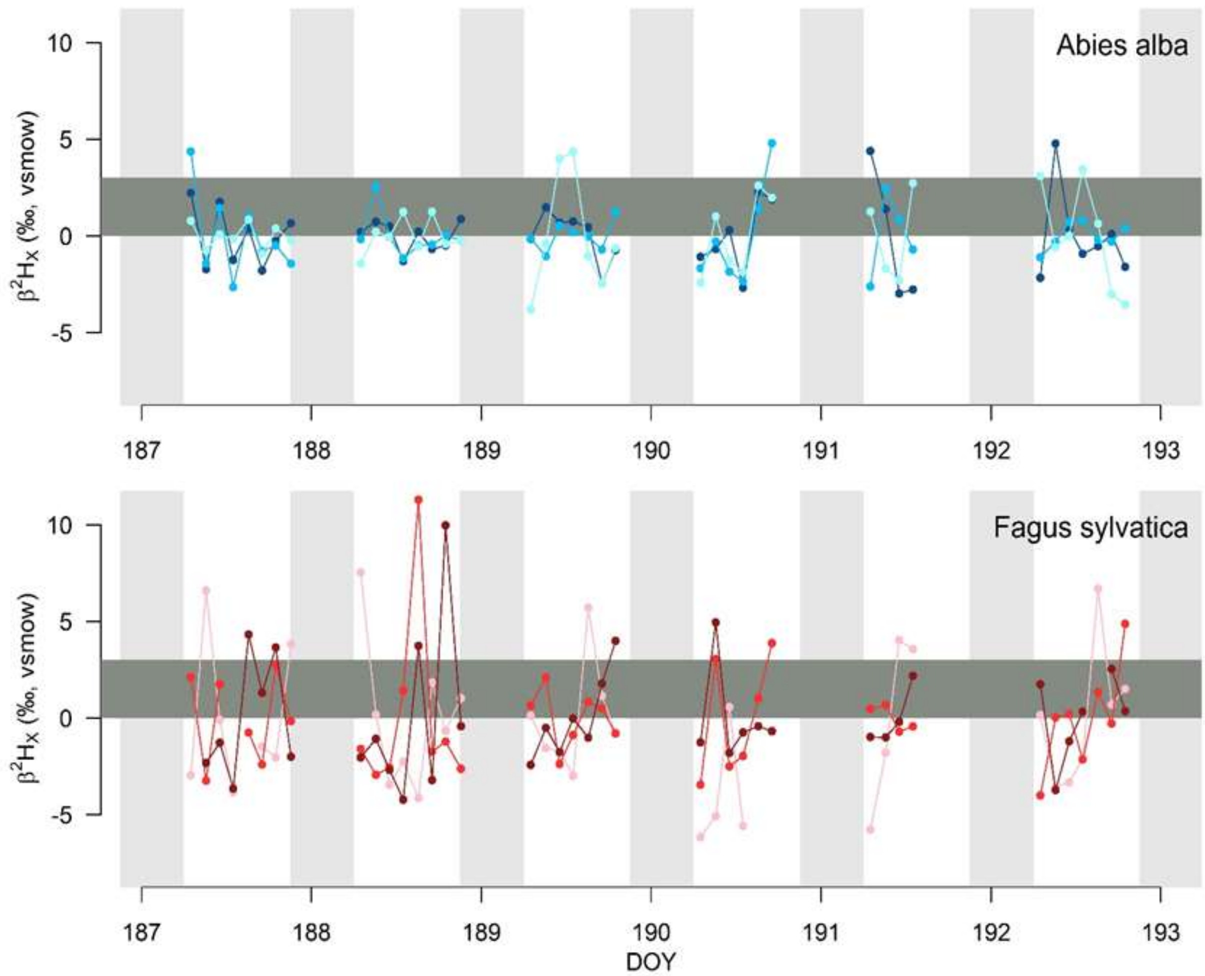

Fig. S5. High temporal field measurements of normalized δ^2H composition of xylem water (β^2H_X) of three *Abies alba* individuals (blue, branch samples) and three *Fagus sylvatica* individuals (red, branch samples) sampled during a drought period in July 2017 in the "Freiamt" field site in south-west Germany. Horizontal dark grey colored envelope delineates the acceptable variance from the stem mean (i.e. 3‰) according to the standard assumption of no variance along the length of a lignified plant. Light grey vertical envelopes mark the nighttime periods.

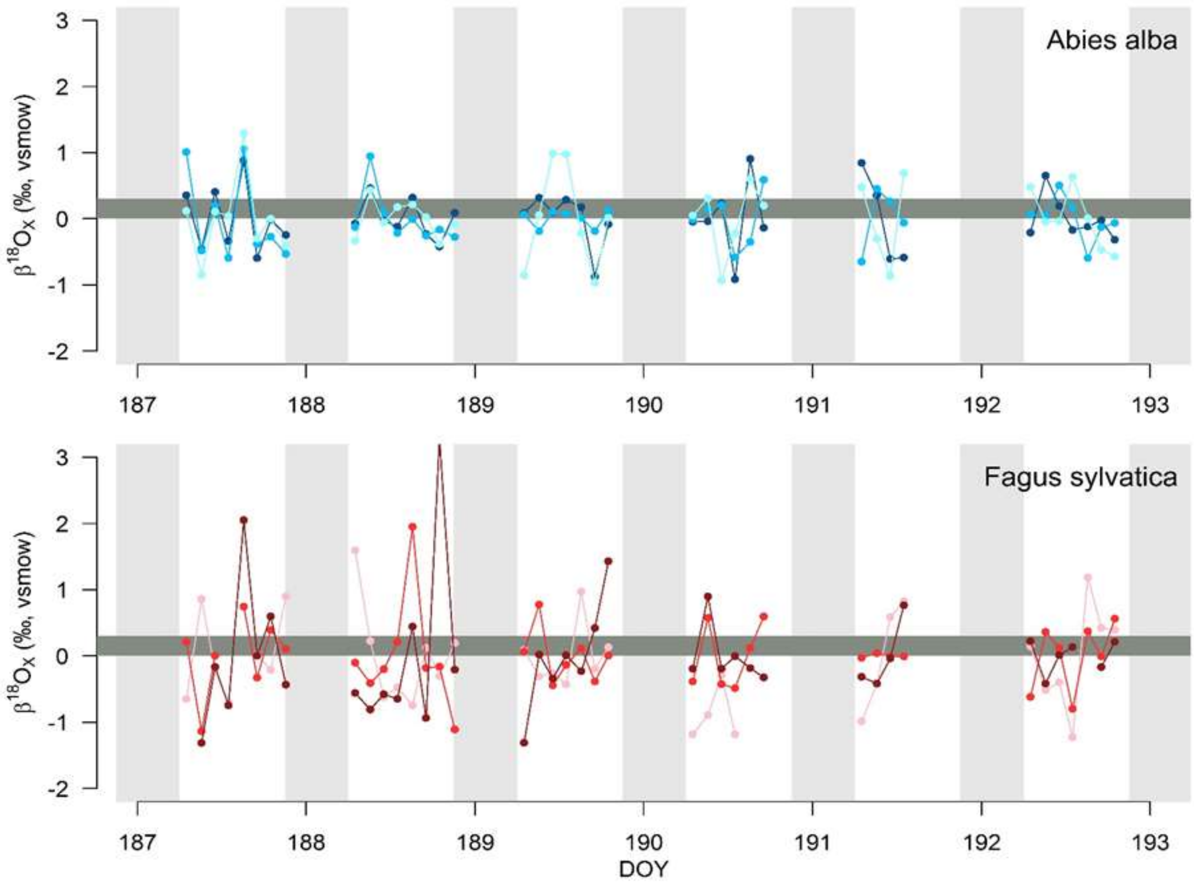

Fig. S6. High temporal field measurements of normalized $\delta^{18}O$ composition of xylem water ($\beta^{18}O_X$) of three *Abies alba* individuals (blue, branch samples) and three *Fagus sylvatica* individuals (red, branch samples) sampled during a drought period in July 2017 in the "Freiamt" field site in south-west Germany. Horizontal dark grey colored envelope delineates the acceptable variance from the stem mean (i.e. 0.3‰) according to the standard assumption of no variance along the length of a lignified plant. Light grey vertical envelopes mark the nighttime periods.

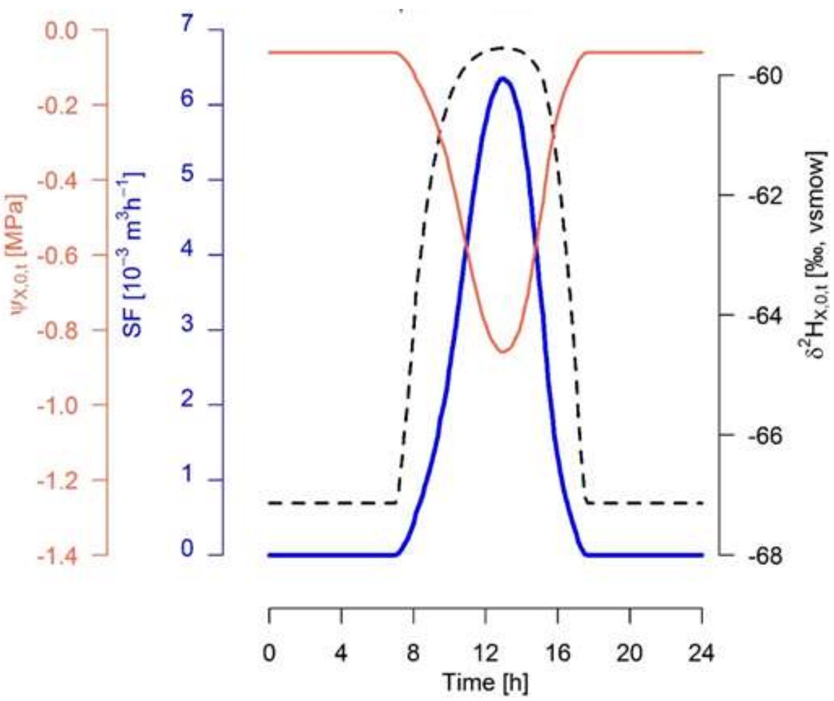

Fig S7: Sap flow rate (*SF*, blue line), δ^2H composition of xylem water at stem base ($\delta^2 H_{X,0,t}$ black dashed line) and water potential at stem base ($\Psi_{X,0,t}$, red line) shown for a single day.

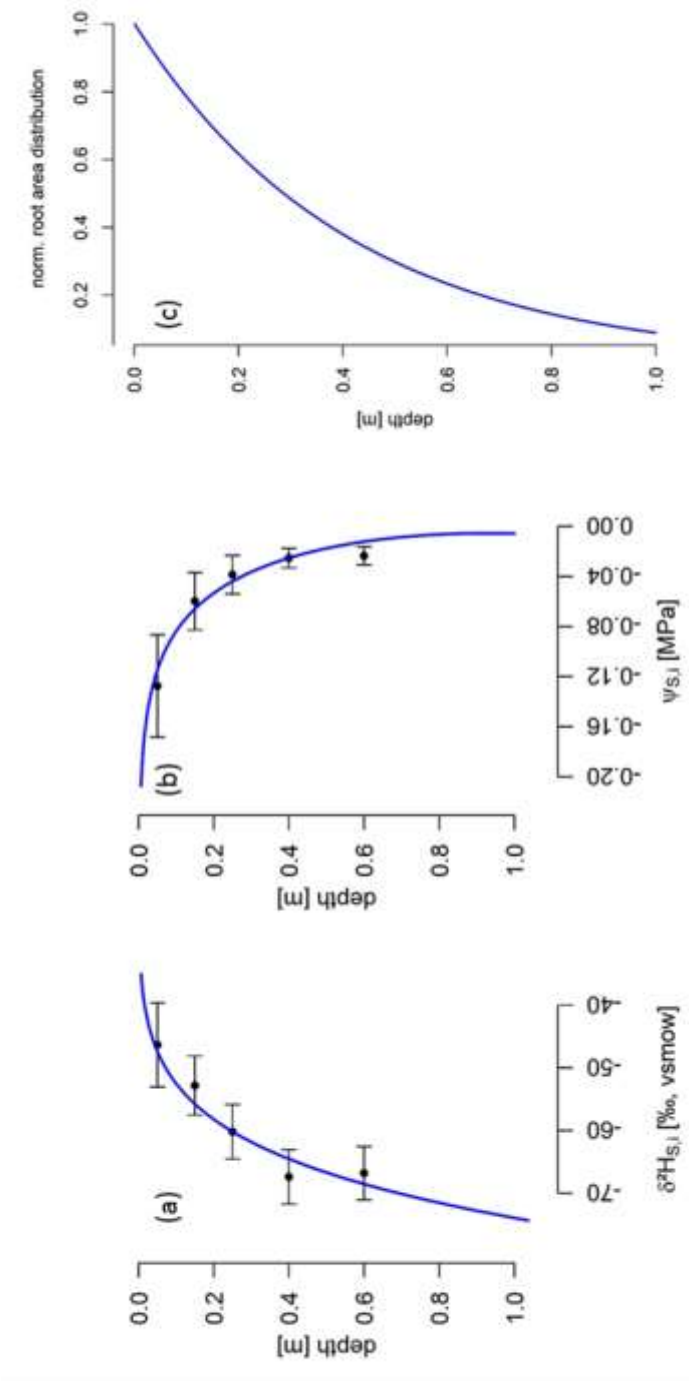

Fig. S8. (a) ^2H composition of soil water ($\delta^2H_{S,i}$) with depth, data from Meißner et al. (2012). **(b)** Soil water potential ($\Psi_{S,i}$) over the soil depth, data from Meißner et al. (2012). **(c)** The relative absorptive root area distribution with soil depths adapted from Jackson et al. (1995) and normalized to the topsoil. All equations and corresponding parameters for the fitted curves can be found in Table S1.

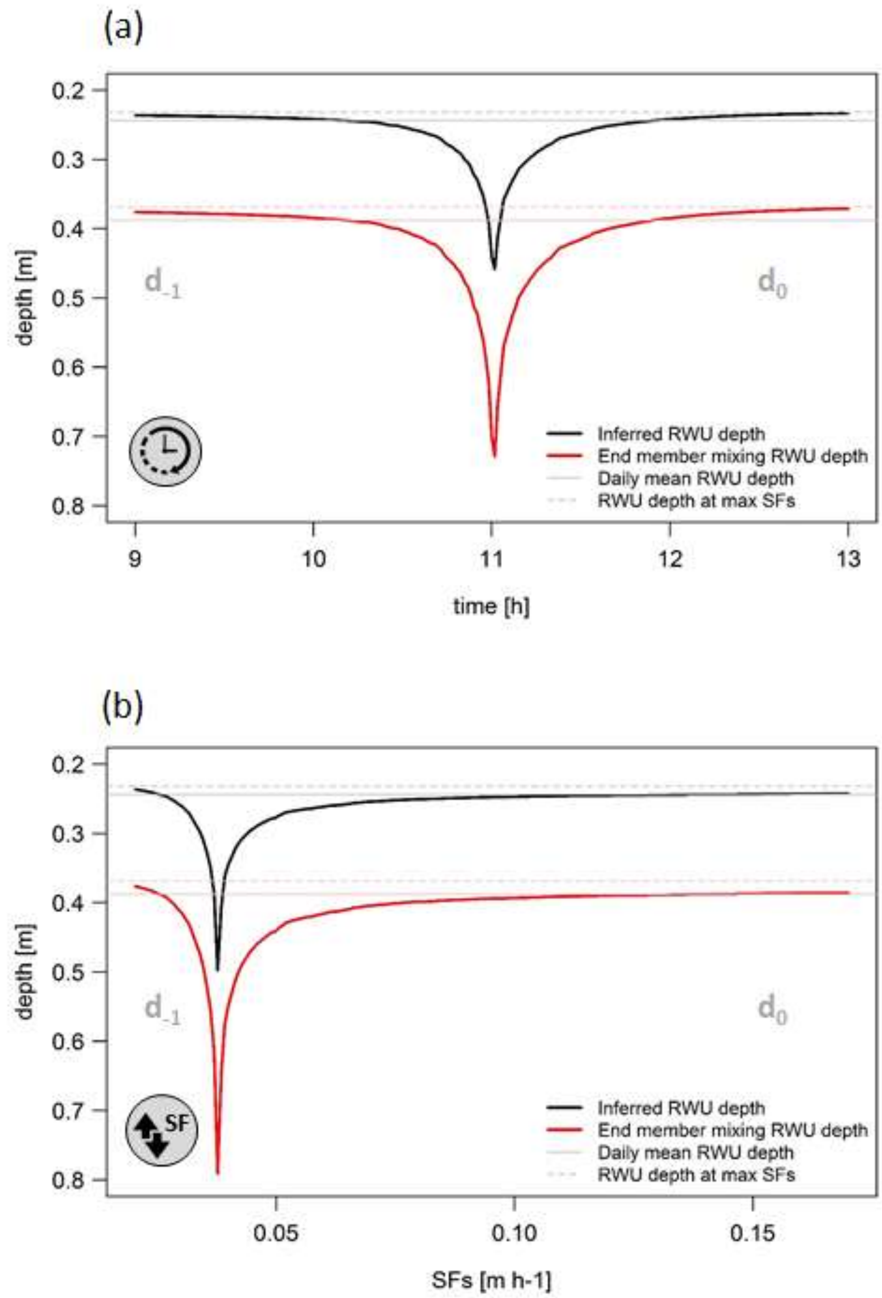

Fig. S9. Differences between the (RWU) depth derived from using either the direct inference (black line) or the end member mixing (red line) approach. **Panel a:** The derived RWU depth for a tree sampled at standard tree coring height (i.e. 1.30 m) having a sap flux density (SF_S) of 0.04 m h^{-1} (i.e. SF_V = 0.28 m h^{-1}), over the common sampling period (9:00 until 13:00). **Panel b:** The derived RWU depth considering a tree sampled at standard tree coring height (1.30 m) at 11:00, but which differs in SF_S. The grey and pink solid lines represent daily mean RWU depth while the grey and pink dashed lines represent the RWU depth at peak sap flow activity, respectively, for the direct inference and end-member mixing model approach. d_{-1} and d_0 indicate whether the derived RWU depth error corresponds to the previous or current day of measurement.

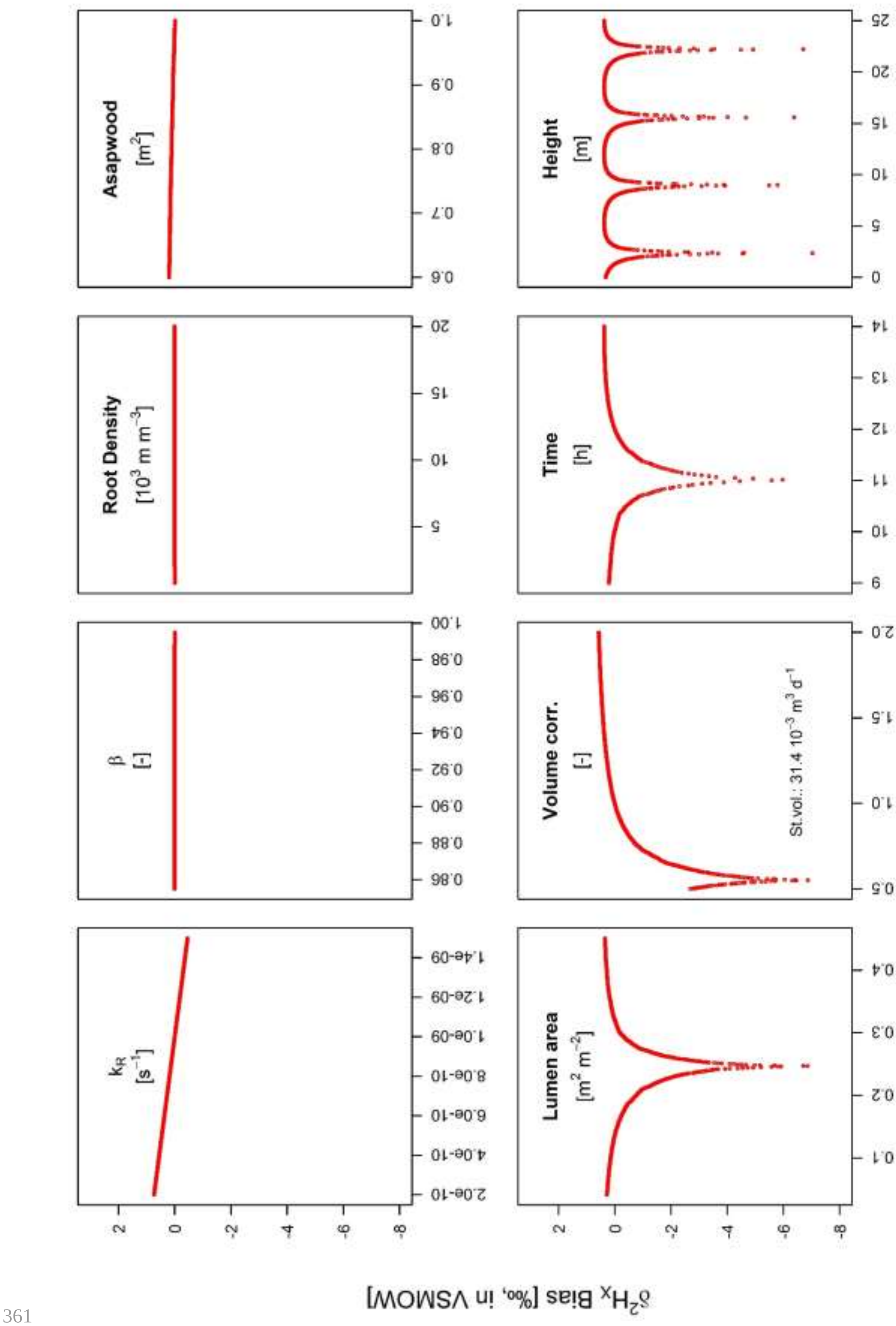
k_R [s^{-1}]
β [-]
Root Density [10^3 m m^{-3}]
Asapwood [m^2]
Lumen area [m^2 m^{-2}]
Volume corr. [-]
St.vol.: 31.4 10^{-3} m^3 d^{-1}
Time [h]
Height [m]
δ^2H_X Bias [‰, in VSMOW]

Fig. S10. Sensitivity analysis where all parameters are varied one-at-the-time as compared to the standard parameterization (see Table S1). For each studied variable, 1000 model runs were performed, studying the resulting δ^2H_X bias in comparison with the standard run. Each time, the studied parameter value was assigned randomly from a defined probability distribution or range using a Latin Hypercube scheme (see Table S2). The effective root radial conductivity (k_R, in s^{-1}), the β (-), and root density (in 10^3 m m^3) together form an informative proxy for the soil to root resistance. The lumen fraction (in m^2 m^{-2}), sapwood area (*Asapwood*, in m^2), and the total diurnal transported sap flow volume, i.e. net root water uptake (Volume corr., factor of standard run volume), provide an informative proxy for the sap flux density. (see Table S1). Time (in h) and height (in m) respectively represent the timing of sampling and the height of sample collection.

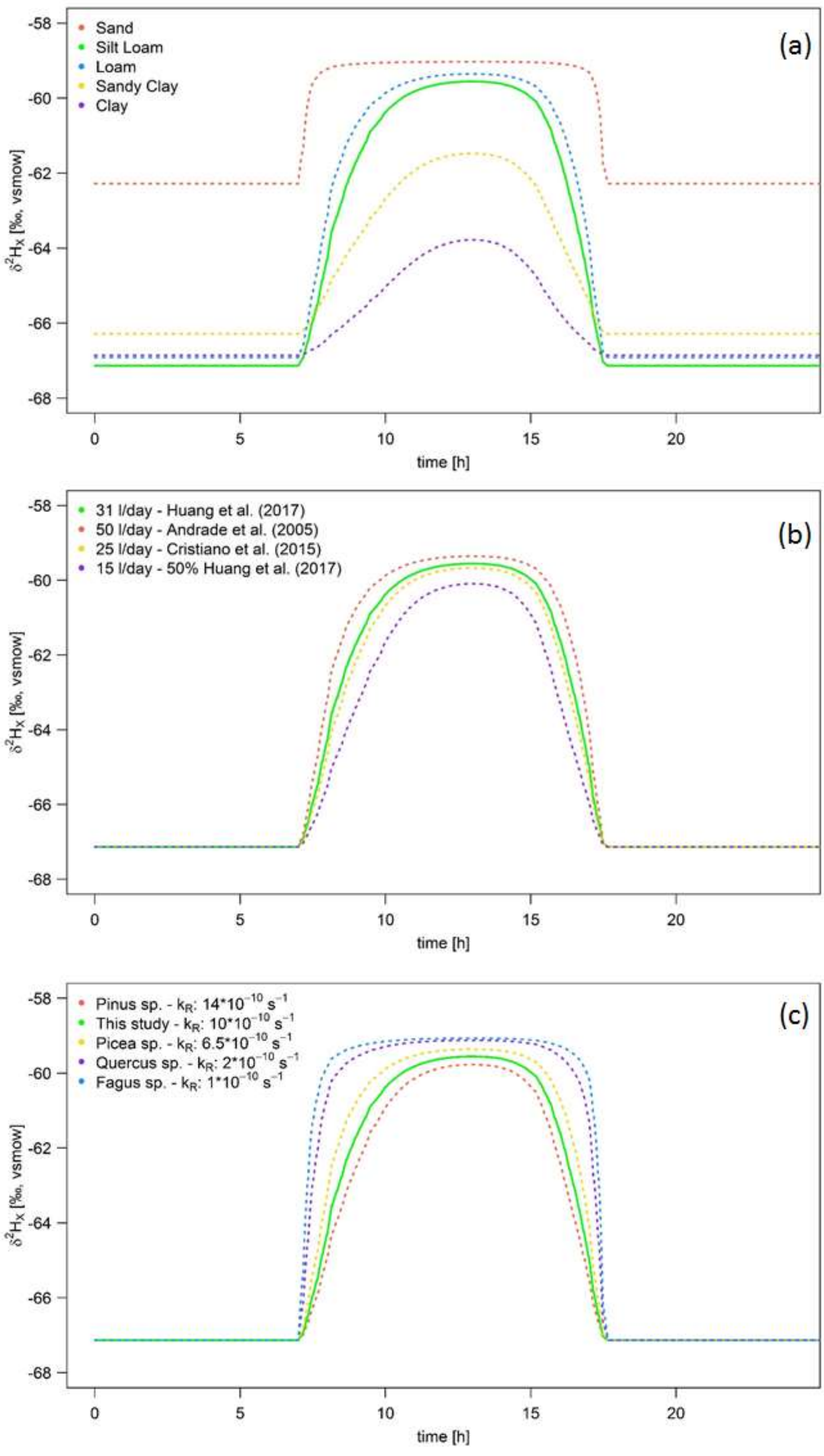

(a)
Sand
Silt Loam
Loam
Sandy Clay
Clay
δ2HX [‰, vsmow]
time [h]
(b)
31 l/day - Huang et al. (2017)
50 l/day - Andrade et al. (2005)
25 l/day - Cristiano et al. (2015)
15 l/day - 50% Huang et al. (2017)
δ2HX [‰, vsmow]
time [h]
(c)
Pinus sp. - kR: 14*10-10 s-1
This study - kR: 10*10-10 s-1
Picea sp. - kR: 6.5*10-10 s-1
Quercus sp. - kR: 2*10-10 s-1
Fagus sp. - kR: 1*10-10 s-1
δ2HX [‰, vsmow]
time [h]

371

Fig. S11. Model sensitivity to (bio)physical parameters. The standard model run is shown by the solid green line in all panels. **Panel a:** fixed soil moisture and depth profile in the isotope composition of soil water ($\delta^2 H_{S,i}$), but with different soil types influencing the soil conductivity and soil water potential gradient in the soil ($\Psi_{S,i,t}$). Parameterization for each soil type is derived from Clapp & Hornberger (1978). **Panel b:** Impact of altering volumes of water taken up by the plant. **Panel c:** Effect of altering values of the effective root radial conductivity (k_R) values. Values are species-specific and are derived from the literature (Leuschner et al., 2004; Rüdinger et al., 1994; Sands et al., 1982; Steudle and Meshcheryakov, 1996). In each panel all other parameters follow the standard plant parameterization (Table S1).

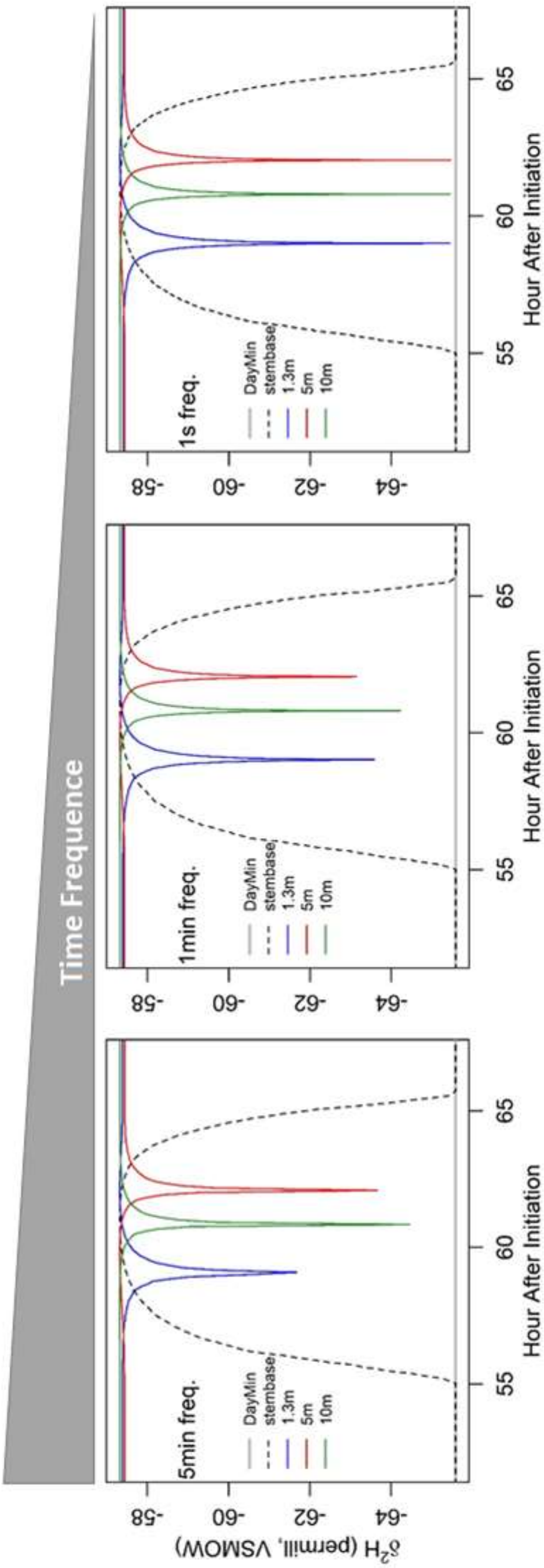

Fig. S12. Model simulations performed with varying temporal resolutions, i.e. 5min, 1min, and 1sec.

Table S1. An overview of the model standard parameterization of the present model, including sap flow, with corresponding references to literature.

Abbr.	Parameter	Unit	Value	Source
A_{Rtot}	The plants' total absorptive root area	m^2	$e^{0.88\cdot\ln\left(\pi\cdot\left[\frac{DBH\cdot 10^2}{2}\right]^2\right)-2}$	Čermák *et al.* (2006) $A_{Rtot} = 23.825\ m^2$
$A_{R,i}$	The absorptive root area distribution over soil layer *i*	m^2	$A_{Rtot} \cdot β^{100\cdot z_i} \cdot (1 - β^{100\cdot Δz})$	A_{Rtot} multiplied by the integrated root distribution of each soil layer adapted from Jackson *et al.* (1996)
			β =0.976	Huang *et al.* (2017)
$A_{SAPWOOD}$	Sapwood area	m^2	$\frac{1.582 \cdot [DBH \cdot 10^2]^{1.764}}{10^4}$	Meinzer *et al.* (2001)
Ax	Total lumen area	m^2	$LF \cdot A_{SAPWOOD}$	
B_i	The overall root length density per unit of soil, not necessarily limited to the studied plant.	$m\ m^{-3}$	$R_0 \cdot β^{100\cdot z_i} \cdot \ln(β)$	Adapted from Huang *et al.* (2017) R_0= -438 688 β =0.976
DBH	Diameter at breast height	m	0.213	Huang *et al.* (2017)
$\delta^2 H_{S,i}$	^2H composition of soil water of the sampled soil layers	in ‰, VSMOW	$a + (z_i + b)^c$	Adapted from Meißner *et al.* (2012) …a: -73.98008 …b=0.001 …c=0.148735;
Δz	The thickness of each soil layer	m	0.001	
f_t	Temporal resolution	s^{-1}	1/60	
k_R	The effective root radial conductivity	s^{-1}	10^{-9}	Huang *et al.* (2017)

Table S1 (continuation)

Abbr.	Parameter	Unit	Value	Source
$K_{S,i}$	The soil hydraulic conductivity defined per soil depth	$m\ s^{-1}$	$K_{s,max} \cdot \left(\frac{\Psi_{sat}}{\Psi_{S,i,t}}\right)^{2+\frac{3}{b}}$	Huang *et al.* (2017)
			$K_{s,max}$= 7.2·10^{-6} $m\ s^{-1}$	Clapp & Hornberger (1978) [Table 2, silt loam soil]
			Ψ_{sat}= -0.786 m H_2O	Clapp & Hornberger (1978) [Table 2, silt loam soil]
			b = 5.30	Clapp & Hornberger (1978) [Table 2, silt loam soil]
LF	Lumen fraction per unit sapwood area	$m^2\ m^{-2}$	0.136	Zanne *et al.* (2010) [Table 2]
SF_t	Instantaneous sap flow at time t	$m^3\ s^{-1}$		Adapted from Huang *et al.* (2017) [derived from scenario 6, day 11]
$\Psi_{S,i,t}$	Water potential at a specific soil layer depth *i* and time *t*	m H_2O	$(a + b \cdot log(z_i) - c \cdot z_i^2) \cdot CT$	Adapted from Meißner *et al.* (2012) a: 19.8455·10^{-3} b: 44.8909·10^{-3} c: 25.5594·10^{-3} CT: 101.97 (i.e. conversion factor between MPa and m H_2O)

z_i the soil depth of the i^{th} soil layer (in m)

Table S2. An overview of the defined distribution and ranges used for the sensitivity analysis whose results are displayed in Fig S10.

Model Variable	Description	Unit	Distribution	Specification
Variables that provide an informative proxy for the soil to root resistance				
k_R	The effective root radial conductivity	s^{-1}	Uniform	St.=$10\cdot10^{-10}$, min = $2\cdot10^{-10}$, max = $15\cdot10^{-10}$
Root density	Integral of B_i for entire soil depth by changing R0 (see Table S1)	m	Uniform	St.= 4000, min = 1000, max = 20000
β	Factor defining root length density profile (see Table S1)	[-]	Uniform	St.= 0.976, min = 0.855, max = 0.995
Variables that provide an informative proxy for the sap flow velocity of a plant				
$A_{SAPWOOD}$	Sapwood area	m^2	Uniform	St.= 0.979, min = 0.6, max = 1
Lumen Fraction	Lumen fraction	$m^2\ m^{-2}$	Uniform	St.=0.136, min = 0.0411, max = 0.451
Volume corr.	Correcting factor of the daily total transported sap flow volume which in the standard run corresponds to $31.4\ 10^{-3}\ m^3$	[-]	Uniform	St.= 1, min = 0.5, max = 2.0
Variables related to the sample collection protocol				
Height	Height of sampling	m	Uniform	St. = 1.3, min = 0, max = 25
Time	Timing of sampling	h	Uniform	St. = 12, min = 9; max = 14

With: *St.* parameter value of the standard run, *min* and *max* the minimum and maximum assigned value

References in figures and tables

Andrade, J. L., Meinzer, F. C., Goldstein, G. and Schnitzer, S. A.: Water uptake and transport in lianas and co-occurring trees of a seasonally dry tropical forest, Trees, 19(3), 282–289, doi:10.1007/s00468-004-0388-x, 2005.

Čermák, J., Ulrich, R., Staněk, Z., Koller, J. and Aubrecht, L.: Electrical measurement of tree root absorbing surfaces by the earth impedance method: 2. Verification based on allometric relationships and root severing experiments, Tree Physiol., 26(9), 1113–1121, doi:10.1093/treephys/26.9.1113, 2006.

Clapp, R. B. and Hornberger, G. M.: Empirical equations for some soil hydraulic properties, Water Resour. Res., 14(4), 601–604, doi:10.1029/WR014i004p00601, 1978.

Cristiano, P. M., Campanello, P. I., Bucci, S. J., Rodriguez, S. A., Lezcano, O. A., Scholz, F. G., Madanes, N., Di Francescantonio, D., Carrasco, L. O. and Zhang, Y.-J.: Evapotranspiration of subtropical forests and tree plantations: A comparative analysis at different temporal and spatial scales, Agric. For. Meteorol., 203, 96–106, 2015.

Huang, C., Domec, J., Ward, E. J., Duman, T., Manoli, G., Parolari, A. J. and Katul, G. G.: The effect of plant water storage on water fluxes within the coupled soil–plant system, New Phytol., 213(3), 1093–1106, doi:10.1111/nph.14273, 2017.

Leuschner, C., Coners, H. and Icke, R.: In situ measurement of water absorption by fine roots of three temperate trees: species differences and differential activity of superficial and deep roots, Tree Physiol., 24(12), 1359–1367, doi:10.1093/treephys/24.12.1359, 2004.

Meinzer, F. C., Goldstein, G. and Andrade, J. L.: Regulation of water flux through tropical forest canopy trees: do universal rules apply?, Tree Physiol., 21(1), 19–26, doi:10.1093/treephys/21.1.19, 2001.

Meißner, M., Köhler, M., Schwendenmann, L. and Hölscher, D.: Partitioning of soil water among canopy trees during a soil desiccation period in a temperate mixed forest, Biogeosciences, 9(8), 3465–3474, doi:10.5194/bg-9-3465-2012, 2012.

Rüdinger, M., Hallgren, S. W., Steudle, E. and Schulze, E.-D.: Hydraulic and osmotic properties of spruce roots, J. Exp. Bot., 45(10), 1413–1425, doi:10.1093/jxb/45.10.1413, 1994.

Sands, R., Fiscus, E. L. and Reid, C. P. P.: Hydraulic properties of pine and bean roots with varying degrees of suberization, vascular differentiation and mycorrhizal infection., Funct. Plant Biol., 9(5), 559–569, doi:10.1071/PP9820559, 1982.

Steudle, E. and Meshcheryakov, A. B.: Hydraulic and osmotic properties of oak roots, J. Exp. Bot., 47(3), 387–401, doi:10.1093/jxb/47.3.387, 1996.

Zanne, A. E., Westoby, M., Falster, D. S., Ackerly, D. D., Loarie, S. R., Arnold, S. E. J. and Coomes, D. A.: Angiosperm wood structure: global patterns in vessel anatomy and their relation to wood density and potential conductivity, Am. J. Bot., 97(2), 207–215, doi:10.3732/ajb.0900178, 2010.